CHEMISTRY & SUSTAINABILITY

CHEMSUSCHEM

ENERGY & MATERIALS

Accepted Article

Title: Synergistic effect of cobalt and iron in layered double hydroxide catalysts for the oxygen evolution reaction

Authors: Fengkai Yang, Kirill Sliozberg, Ilya Sinev, Hendrik Antoni, Alexander Bähr, Kevin Ollegott, Wei Xia, Justus Masa, Wolfgang Grünert, Beatriz Roldan Cuenya, Wolfgang Schuhmann, and Martin Muhler

To be cited as: *ChemSusChem* 10.1002/cssc.201601272

Link to VoR: http://dx.doi.org/10.1002/cssc.201601272

A Journal of

ChemPubSoc Europe

WILEY-VCH

www.chemsuschem.org

Synergistic effect of cobalt and iron in layered double hydroxide catalysts for the oxygen evolution reaction

Fengkai Yang[a], Kirill Sliozberg[b], Ilya Sinev[c], Hendrik Antoni[a], Alexander Bähr[a], Kevin Ollegott[a], Wei Xia[a], Justus Masa[b], Wolfgang Grünert[a], Beatriz Roldan Cuenya[c], Wolfgang Schuhmann[b], and Martin Muhler[a]
[a] Laboratory of Industrial Chemistry, Universitätsstr. 150, Ruhr-University Bochum, D-44780 Germany
[b] Analytical Chemistry and Center for Electrochemical Sciences (CES), Universitätsstr. 150, Ruhr-University Bochum, D-44780 Germany
[c] Department of Physics, Universitätsstr. 150, Ruhr-University Bochum, D-44780 Germany

Abstract
Co-based layered double hydroxides (LDH) catalysts with Fe and Al contents in the range from 15 to 45 at% were synthesized by an efficient co-precipitation method. In these catalysts, Fe^{3+} or Al^{3+} ions play an essential role as trivalent species to stabilize the LDH structure. The obtained catalysts were characterized by a comprehensive combination of surface- and bulk-sensitive techniques and evaluated for the oxygen evolution reaction (OER) on rotating disk electrodes. The OER activity decreased with increasing Al content for the Co- and Al-based LDH catalysts, whereas a synergistic effect in Co- and Fe-based LDHs was observed resulting in an optimal Fe content of 35 at%. This catalyst was spray-coated on Ni foam electrodes and showed very good stability in a flow-through cell with a potential of ca. 1.53 V at 10 mA/cm^2 in 1 M KOH for at least 48 h.

Introduction
In the last decade, water electrolysis, which converts intermittently available renewable energy into H_2, has drawn a lot of attention due to the increasing global energy demand.[1] Its key challenge is the high overpotential required to reach the solar flux equivalent current density (e.g., 10 mA/cm^2), which mainly results from the sluggish oxygen evolution reaction (OER) due to its four-electron transfer pathway.[1,2] For this reason, suitable OER catalysts have to be applied to lower the overpotential thereby increasing the water oxidation efficiency. Materials such as RuO_2 and IrO_2 are known to be the most active OER catalysts under acidic conditions.[3] However, their scarcity and high costs limit their application on a large scale. In comparison, Co-based materials are known to be promising OER catalysts in alkaline

electrolytes, and are thus more appealing for large-scale use due to their high abundance on earth and the low cost of cobalt.[4]

To study the nature of self-assembled Co-based OER active centers, numerous efforts have been undertaken focusing on Co-Pi catalysts electrodeposited from a phosphate-containing electrolyte.[5–10] It is widely accepted that Co-Pi catalysts consist of amorphous hydrated cobaltates mainly in the Co^{3+} oxidation state as deposited and partly in the Co^{4+} state under reaction conditions.[5,7,10] Further structural studies indicate that Co-Pi catalysts are built of fragments containing CoO_6 octahedra,[6] which are further assembled in the form of a layered structure intercalated with anions.[8,9,11] For the heterogeneous Co-based OER catalysts, however, conflicting conclusions have been reported. Yeo and Bell[12] suggested that the OER activity should be promoted by $Co^{3+/4+}$ sites based on their study of a gold-supported thin layer of Co_3O_4. In contrast, it was independently reported by Bao et al.[13] and Xu et al.[14] that the OER activity was improved by oxygen vacancies in Co_3O_4 nanosheets with Co in a lower oxidation state. These conflicting findings can become compatible if a recently proposed mechanism is taken into account assuming that active species on Co_3O_4 surfaces are formed *in situ*, and that tetrahedral Co^{2+} sites are more suitable than octahedral Co^{3+} in a Co_3O_4 spinel structure for the formation of active species under working conditions.[15] Similar to Co-Pi catalysts, the *in situ* formed OER-active species on Co-based heterogeneous catalysts consist of hydrated cobaltate fragments in a layered structure.[16,17] Until now, hydrated cobaltates have been detected under working conditions by means of different *in situ* techniques on the surfaces of various Co-based heterogeneous catalysts including perovskite,[18] phosphate salt[16] CoO,[17] and Co_3O_4.[19] Thus, studies on both electrodeposited Co-Pi and Co-based heterogeneous catalysts point to the dependence of the intrinsic OER activity on Co (oxy)hydroxides in layered structures.

Layered double hydroxides (LDHs) consist of positively charged layered hydroxide sheets formed by tilted edge-sharing MO_6 octahedra and negatively charged counterions (NO_3^-, CO_3^{2-}, etc) in the interlayers. Therefore, LDHs have the closest structural similarity to the *in situ* formed Co-based OER-active species. Recently, Boettcher and co-workers[20] observed a synergistic effect between Co and Fe by electrodepositing a series of hydroxides with different Co:Fe ratio, which is consistent with other works on electrodeposited CoFe-based LDHs showing that the presence of Fe ions significantly promotes the activity of Co-based LDH OER catalysts.[21,22] However, it is difficult to precisely control the Co:Fe ratio in electrochemically deposited thin film catalysts due to the differing deposition kinetics. In this work, we synthesized CoFe- and CoAl-based LDH catalysts with Fe and Al contents in the

range from 15 to 45 at% by an efficient co-precipitation method. In these catalysts, Fe^{3+} or Al^{3+} play an essential role as trivalent species to stabilize the LDH structure. The obtained catalysts were characterized by a comprehensive combination of surface- and bulk-sensitive techniques and evaluated for OER activity on rotating disk electrodes (RDE). The OER activity decreased with increasing Al content for the CoAl-based LDH catalysts, whereas a synergistic effect in CoFe-based LDHs was observed for an optimal Fe content of 35 at%. This catalyst was spray-coated on Ni foam electrodes and tested for long-term stability showing very good stability with a potential of ca. 1.53 V vs. RHE at 10 mA/cm^2 in 1 M KOH at least for 48 h.

Results and discussion

Four CoAl and five CoFe LDH catalysts were prepared in varied Co to Al/Fe ratios by co-precipitation at pH 9 using a 2 M/0.3 M $NaOH/Na_2CO_3$ solution as precipitating agent (see experimental section for more details) followed by drying at room temperature and grinding in a mortar. The obtained catalysts were designated as CoAl*m* and CoFe*n*, with *m* and *n* as the Al or Fe atomic content, respectively. As summarized in Table S1, the Co and Al/Fe contents were quantified by inductively coupled plasma optical emission spectrometry (ICP-OES). Generally, the determined Al or Fe contents were consistent with the nominal values of both CoAl and CoFe LDHs, thus demonstrating the complete co-precipitation of Co^{2+} and Al^{3+}/Fe^{3+} ions at pH 9. In some of the samples, small differences between the nominal and experimentally determined Al/Fe content (max. 0.85 at%) were observed, which can be attributed to experimental errors during the synthesis.

The obtained samples were characterized by X-ray diffraction (XRD) to determine the dependence of the structural properties on the Al/Fe content. As shown in Figure 1(a), all CoAl LDH samples exhibited the reflections at around 11.5° and 23°, which are the characteristic (003) and (006) reflections of the $Co(OH)_2$ LDH structure.[23] Each reflection can be assigned to the reference pattern of pure $Co(OH)_2$ LDH indicating that the LDH was the only crystalline product. A closer look at the patterns of CoAl LDHs reveals that the CoAl LDH samples possess slightly higher 2θ values between 11.5° and 11.9° compared with the (003) reflection at 11.0° in the reference pattern, indicating a smaller interlayer distance between the hydroxide layers in the CoAl LDHs. Interestingly, the 2θ values of the (003) reflection in CoAl LDHs increased gradually from 11.5° to 11.9° with higher Al content above 25 at%. This observation can be attributed to a smaller interlayer distance, which may result from the larger fraction of Al^{3+} with smaller ionic radius in the hydroxide layer and the

stronger electronic attraction between more positively charged hydroxide layers with higher Al content and counter anions in the interlayer. In addition, the CoAl15 and CoAl45 samples had a significantly higher full width at half maximum (FWHM) of the reflections than the other samples with medium Al content demonstrating that smaller crystalline domains were formed with either too high or too low Al^{3+} concentrations. In other words, the LDH structure cannot be sufficiently stabilized with low Al^{3+} concentrations, whereas high Al^{3+} concentrations lead to disordered LDH hydroxide layers presumably due to the different radii of the Co^{2+} and Al^{3+} ions. Similar to CoAl LDHs, the CoFe samples exhibited typical patterns of LDH structures for Fe contents from 15 to 45 at% (Figure 1(b)). With increasing Fe content, the (003) reflections shifted slightly to higher 2θ values from 11.5° to 11.6°. Unlike the CoAl samples, CoFe LDHs showed much smaller changes in both 2θ and FWHM values with increasing Fe content, which is attributed to the more similar ionic radii of Co and Fe ions in the hydroxide layer. Therefore, the CoFe LDHs can be formed with good crystalline structure with less disorder over a wide range of Fe concentrations.

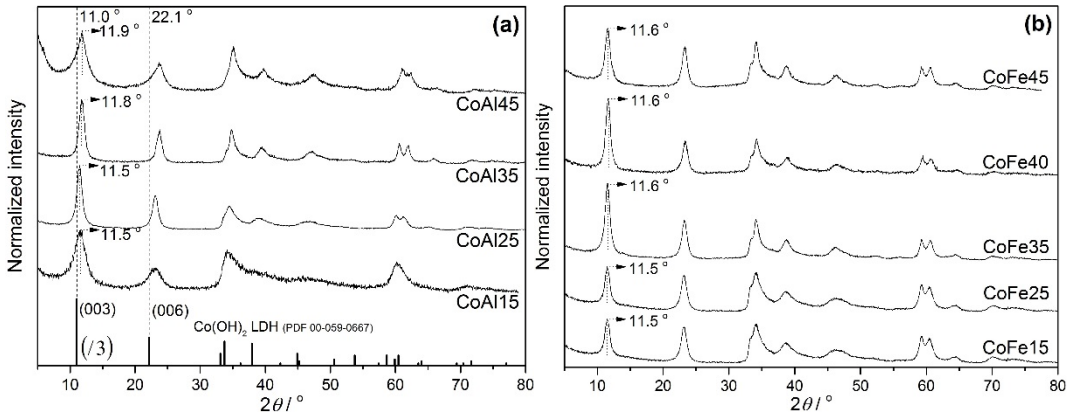

Figure 1. XRD patterns of (a) CoAl and (b) CoFe samples with varied Co^{2+} to M^{3+} ratios.

The Raman spectra of the CoAl and CoFe LDHs are displayed in Figure 2. As shown in Figure 2(a), the asymmetric band at 476 cm^{-1} and the most intense band at 521 cm^{-1} were observed for the CoAl samples. It was reported that similar bands occurred at 462 and 521 cm^{-1} for hydrotalcite-like CoAl LDH[24] and at 457 and 523 cm^{-1} for brucite-like $Co(OH)_2$.[25] Perez-Ramirez et al.[24] assigned the two bands to hydroxyl groups mainly associated with Al and both bands were influenced by probably one divalent cation in its coordination. In contrast, Yang et al.[25] assumed that the two bands were correlated with Co-O symmetric stretching and O-Co-O bending modes, respectively. In this work, the band at 476 cm^{-1} decreased dramatically leaving small symmetric bands, and the band at 521 cm^{-1} almost

disappeared with higher Al content. These observations suggest that the band at 476 cm^{-1} can be assigned to the hydroxyl groups coordinated to Al^{3+}, whereas the band at 521 cm^{-1} as well as the band at around 450 cm^{-1}, which slightly overlaps with the band at 476 cm^{-1}, are correlated with the hydroxyl groups bound to Co^{2+} and strongly influenced by its coordination. In addition, another band was observed at 1057 cm^{-1} for CoAl LDHs, which is assigned to OH bending vibrations.[24,25] Similar to the CoAl LDHs, the CoFe samples showed symmetric bands at 454 and 521 cm^{-1} for low Fe contents (Figure 2(b)). With increasing Fe content, both bands decreased significantly and were hardly observed when the Fe content was above 30 at%. This finding confirms the assignments of the bands at 454 and 521 cm^{-1} to the hydroxyl vibrations of the CoFe LDHs, which is in good agreement with the observations made for CoAl LDHs. Interestingly, the band at 1057 cm^{-1} was hardly detected in any of the CoFe LDH samples. Since one OH^- anion is shared by three $Co(OH)_6$ octahedra in a $Co(OH)_2$ layer,[9] the Raman bands at 454 and 521 cm^{-1} actually originate from OH^- groups bound to 3 Co^{2+} cations. This configuration is statistically rarely formed with an Al^{3+} or Fe^{3+} content of more than 33 at%, leading to a significant decrease in Raman intensities at 454 and 521 cm^{-1} for the samples CoM35, CoM40 and CoM45.

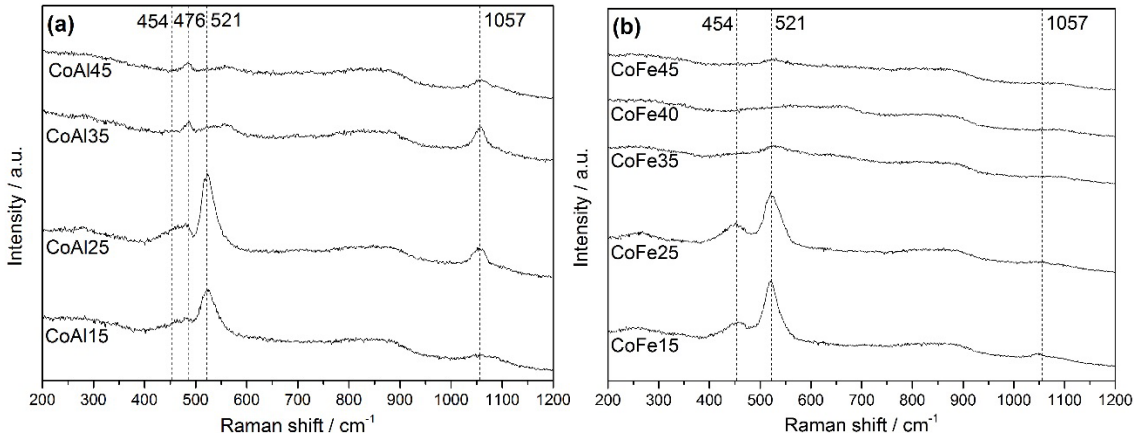

Figure 2. Raman spectra of (a) CoAl and (b) CoFe samples with varied Co^{2+} to M^{3+} ratios.

The thermal decomposition of the CoAl35 and CoFe35 LDHs was studied by thermogravimetric analysis coupled with mass spectrometry (TG-MS). As shown in Figure 3(a), CoAl35 underwent significant decomposition in 5 vol% O_2/He above 50 ^oC showing one small shoulder at 92 ^oC and two intense peaks at 172 and 242 ^oC in the differential thermogravimetric analysis (DTG) profile, which are in good agreement with reported TG studies on CoAl LDH.[24,26] Taking the MS profiles into account, the DTG peak at 172 ^oC is correlated to the release of H_2O (m/z=18) at 185 ^oC, whereas the DTG peak at 242 ^oC is due

to the formation of both H_2O and CO_2 (m/z=44) at ca. 250 °C. In comparison, the CoFe35 sample decomposed upon heating resulting in three intense DTG peaks at 147, 185 and 393 °C (Figure 3(b)). The MS profiles show that the most intense mass loss at 147 °C originates from dehydration with a strong m/z=18 signal at 155 °C. The mass loss peak at 185 °C results mainly from the release of both H_2O (m/z=18) at 189 °C and CO_2 (m/z=44) at 199 °C. The mass loss at 393 °C, which is only observed for CoFe35, can be assigned to either NO_3^- decomposition with a significant formation of NO (m/z=30) at 375 °C or the thermal decomposition of $Co_{0.65}Fe_{0.35}O_x$ containing Fe^{3+} to the $FeCo_2O_4$ spinel containing Fe^{2+} leading to the release of O_2. The latter speculation is supported by the observation that a lower temperature was observed for the third DTG peak when heating CoFe35 in pure He (Figure S1).

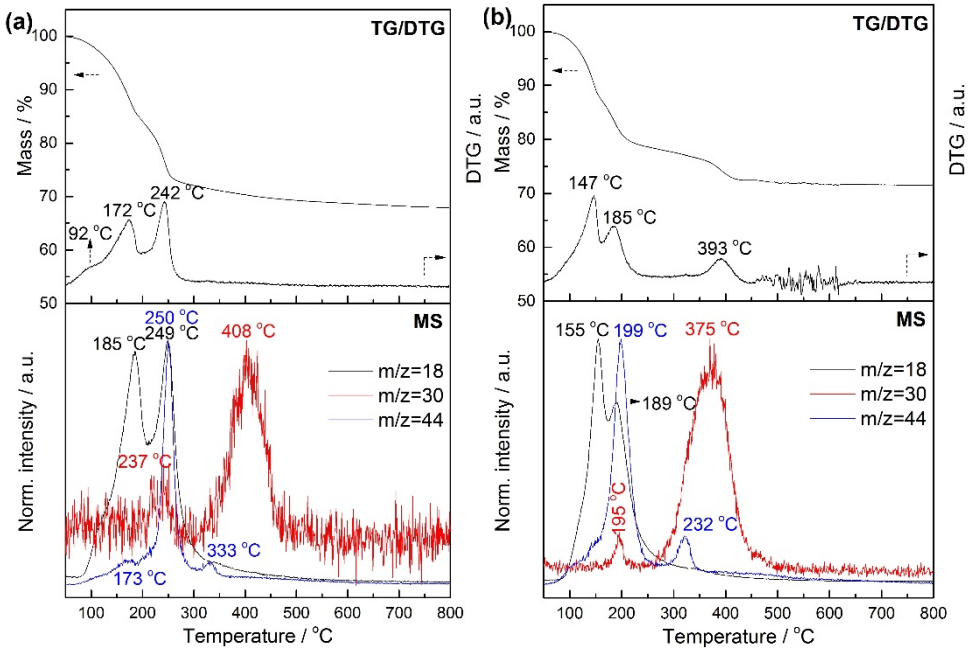

Figure 3. TG-MS profiles of the (a) CoAl35 and (b) CoFe35 samples using a heating rate of 5 K/min to 800 °C in 5 vol% O_2/He.

The temperature-programmed reduction (TPR) profiles of the CoAl and CoFe LDHs are displayed in Figure 4. CoAl LDHs were hardly reduced up to 300 °C, and in the temperature range from 300 °C to 700 °C only broad and weak H_2 consumption peaks were detected. This observation is consistent with the reported TPR profiles of non-calcined CoAl LDHs, for which the presence of the Al^{3+} ions led to incomplete reduction of Co^{2+}.[27] With increasing Al content, the H_2 consumption peak shifted to higher temperature from 434 °C for CoAl15 to 548 °C for CoAl45, demonstrating the detrimental effect of more Al on the reducibility of Co.

In comparison, the CoFe samples showed more defined reduction profiles between 300 and 500 °C. The H_2 consumption maximum shifted gradually from about 372 °C to 401 °C with increasing Fe content. However, the individual reduction of the Co and Fe ions cannot be distinguished in the TPR profiles. The shift of the H_2 consumption peak is in good agreement with the reported TPR profiles of bimetallic $CoFeO_x$, which showed a higher reduction temperature of FeO_x compared with CoO_x.[28] Taking the TG-MS study into account, which monitored strong dehydration and decarboxylation processes below 250 °C, the main H_2 consumption by CoAl and CoFe LDHs in the TPR profiles between 300 and 500 °C most probably results from the reduction of oxide species mixed with anions formed by thermal decomposition.

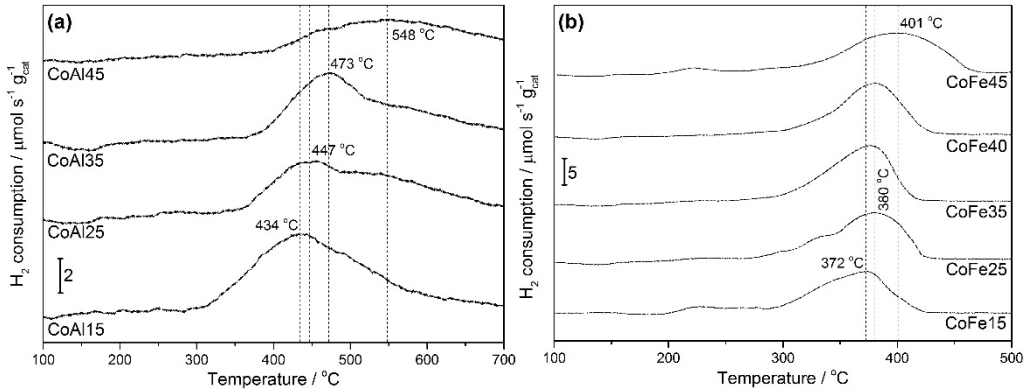

Figure 4. TPR profiles of (a) CoAl and (b) CoFe samples with varied Co^{2+} to M^{3+} ratios.

The X-ray photoelectron (XP) spectra of selected CoFe LDHs were recorded and are displayed in Figure 5. In the C 1s spectra, aliphatic and carbonate species were detected at 284.5 and 288.6 eV, respectively (Figure 5(a)). CO_3^{2-} was introduced to stabilize the LDH structure as counter anions in the interlayers. The deconvoluted O 1s spectra consist of two oxygen species at 529.3 and 530.9 eV, which can be assigned to oxide-like and hydroxide-like oxygen species, respectively (Figure 5(b)).[20] In addition, the spectra of oxide-like oxygen species increased significantly with higher Fe content, confirming the correlation between Fe^{3+} and O^{2-} species. The Fe 2p spectrum with a maximum at 711 eV is similar to previously reported spectra of FeOOH (Figure 5(c)).[29] The Co 2p spectra did not change with varied Fe content. The intense satellite at 785.2 eV indicates that the Co species were mainly in the Co^{2+} oxidation state.

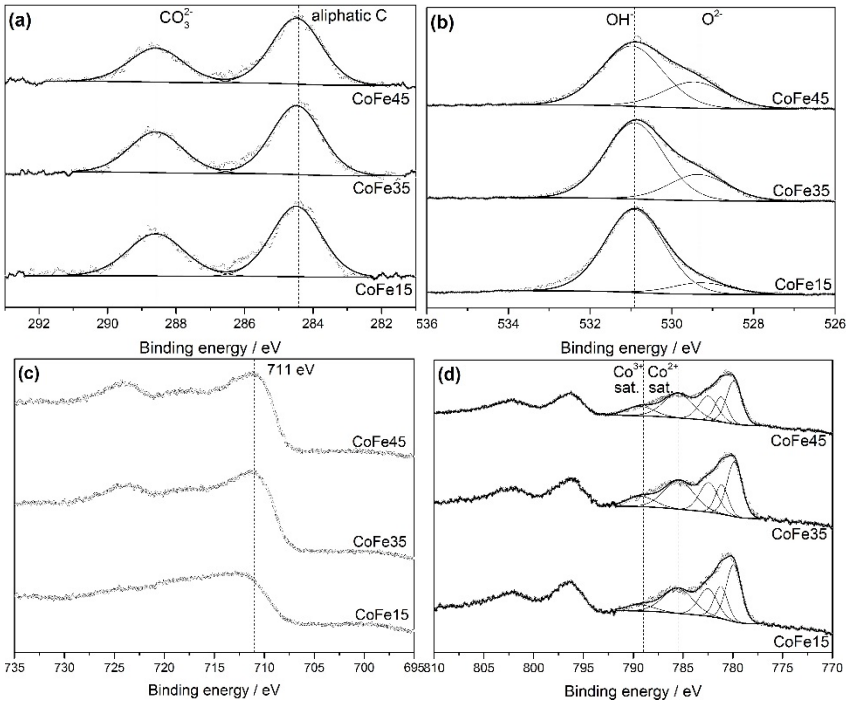

Figure 5. XP spectra of (a) C 1s, (b) O 1s, (c) Fe 2p and (d) Co 2p of selected CoFe samples.

To obtain more insight in the local coordination geometry of the metal ions, X-ray fine structure absorption spectroscopy (XAFS) was performed using selected CoFe LDHs at both Fe and Co *K* absorption edges. Fe-*K* X-ray absorption near edge structure (XANES) spectra did not change with different Fe:Co ratio, showing a pre-edge feature at 7113.8 eV, an intense peak above the edge at 7132.6 eV (so-called white line, WL) and two features in the post-edge region at ca. 7139.9 and 7148.4 eV (Figure S2(a)). The overall shape of the XANES spectra does not follow any of those of the reference iron oxides (Figure S3(a)). The pre-edge peak position and intensity, however, indicate a dominance of Fe^{3+} species in 6-fold coordination according to the pre-edge features of crystalline Fe^{2+}- and Fe^{3+}-containing compounds as observed by Wilke et al.[30] A similar shape of the Fe-*K* XANES spectra was recently reported for mixed NiFe oxyhydroxides.[31,32] Similar to the Fe *K*-edge, Co *K*-edge XANES spectra show only insignificant differences (Figure S2(b)). By comparing them to reference spectra (Figure S3(b)), it can be concluded that Co is dominantly in the Co^{2+} state, which is consistent with the Co 2p XP spectra.

Further results on Fe *K*-edge and Co *K*-edge extended X-ray absorption fine structure (EXAFS) spectra of the selected CoFe LDHs are displayed in Figure 6. At both edges, the spectra are dominated by intense backscattering features at 1.45/1.62 Å (Fe *K*- and Co *K*-edge, respectively, not corrected for phase shift) and at 2.69 Å (uncorrected), which likely correspond to metal to oxygen and metal to metal backscattering in a hydroxide structure. It is

particularly remarkable that the intensity of the metal to metal feature in the Fe-*K* EXAFS decreases with increasing iron content, whereas the intensity changes of the first peak assigned to Fe-O are less strong, following the same trend though. In contrast, there is no well-defined trend in the Co *K*-edge EXAFS spectra, with more intense features observed for the CoFe35 sample.

To obtain a deeper understanding of the local coordination of Co^{2+} and Fe^{3+}, EXAFS spectra were fitted using structural models built using the orthorhombic $Co(OH)_2$ structure[33] with Co^{2+} and Fe^{3+} occupying equal crystallographic positions with an atomic ratio of 1:1 (Figures S4 and S5). For each spectrum, M-O and M-M (M = Fe, Co) shells were fitted. An attempt was made to fit the feature at 2.69 Å with both M-Fe and M-Co coordination, but due to the close atomic number of Co and Fe, unreasonable results were obtained. Thus, the Fe-O coordination number (CN) changes from ~5.8 to ~5.5 with increasing iron content from 15 to 35 at% and further to ~5.2 for the sample with 45 at% Fe, whereas the Fe-M CN undergoes more significant changes from ~5.0 to ~4.2 and finally to ~3.9 (see Table S2 for details). The best model fit of the Co *K*-edge EXAFS spectra shows that the highest Co-O and Co-M CNs for the CoFe35 sample are 4.57 and 7.67, respectively (see Table S3), while the other two samples share close Co-M CNs of 7.35 and 7.26 for CoFe15 and CoFe45, respectively. This analysis seems to suggest that the Fe^{3+} ions may prefer to be located at the edges of the LDH platelets with increasing Fe content, whereas the Co^{2+} ions might be located more in the center of the platelets.

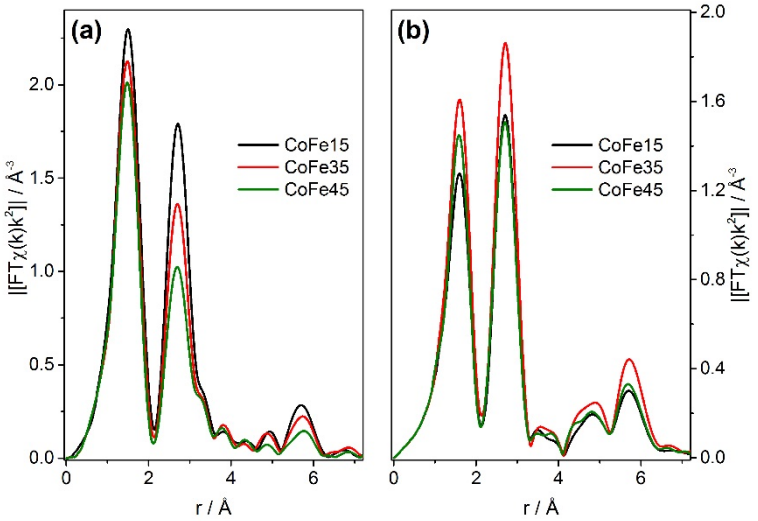

Figure 6. (a) Fe and (b) Co *K*-edge EXAFS spectra of CoFe15, CoFe35 and CoFe45.

The OER activities of the CoAl and CoFe LDHs were determined by drop-coating a suspension of the catalysts on glassy carbon rotating disc electrodes (GC RDE, 3.8 mm diameter) to form thin films. As shown in Figure 7(a), the OER activity decreased with increasing Al content from 15 to 45 at%, corresponding to an increase of the potential at 10 mA/cm^2 from 1.63 to 1.68 V vs. RHE, respectively, indicating that the presence of Al^{3+} ions suppressed the OER activity by diluting the Co sites in CoAl LDHs. A further possible explanation of the diminished activity with increasing Al content could be an effective drop of the charge transfer rate through the catalyst bulk. Considering redox-hopping-type conduction and the presence of mixed $Co^{2+/3+}$ valencies,[34] insertion of the electrochemically inactive Al^{3+} ions in the crystal lattice disables redox-hopping, and the minimal distance for an electron to overcome would be the distance between two Co ions separated by an Al^{3+} ion. Since this distance is much larger than the one between two adjacent Co ions, the charge transfer rate drops in accordance with the Marcus theory.[35] In contrast to Al^{3+}, Fe^{3+} is a redox-active species, which can participate in the redox-hopping-type charge transfer along with Co. CoFe LDHs showed much better OER activities in comparison to the CoAl LDHs with potentials at 10 mA/cm^2 between 1.58 and 1.68 for all the samples. The activity first increased with increasing Fe content up to 35 at% Fe and then decreased with further increase of the Fe content. Thus, an optimal Fe content of 35 at% was derived for the CoFe LDHs (Figure 7(b)).

The Tafel plots showed similar trends as the polarization curves. As shown in Figure 7(c), the Tafel slope increased continuously from 64 mV/decade for CoAl15 to ca. 83 mV/decade for CoAl25 and CoAl35, and finally to 102 mV/decade for CoAl45. In contrast, the Tafel slope of CoFe LDHs decreased significantly from 70 mV/decade for CoFe15 to 49 mV/decade for CoFe35, and then further decreased slightly to 47 mV/decade for CoFe45 (Figure 7(d)). The overpotentials at 10 mA/cm^2 and Tafel slopes of CoAl and CoFe LDHs are summarized in Figure 7(e). Both the overpotentials at 10 mA/cm^2 and the Tafel slopes of the CoAl catalysts increased with rising Al content. Although the presence of Al^{3+} was necessary for maintaining the LDH structure, it appears that the sites occupied by Al^{3+} do not participate in the OER. Instead, such sites inhibit the reaction due to the substitution of catalytically active Co sites. In contrast, the CoFe catalysts exhibit a volcano-like plot in both the overpotentials at 10 mA/cm^2 and the Tafel slopes as a function of the Fe content in the catalysts. The optimal Fe content was around 35 at%, suggesting a synergistic interaction between the Fe and Co ions during the OER.

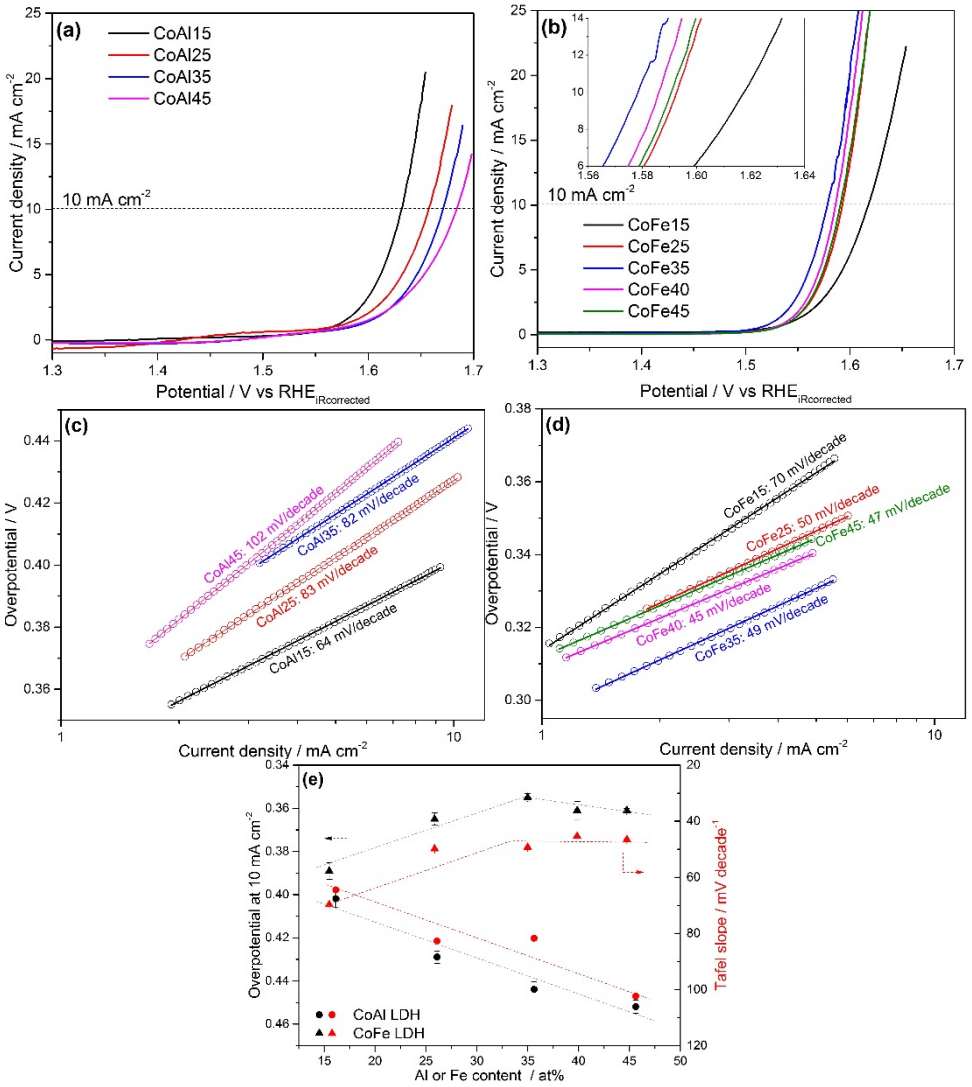

Figure 7. OER activities of (a) CoAl and (b) CoFe samples; Tafel slopes of (c) CoAl and (b) CoFe samples; (e) overpotential at 10 mA/cm^2 and Tafel slopes of the catalysts vs. Al/Fe atomic content determined by ICP-OES.

Table 1 summarizes the OER activities reported in literature demonstrating that the results obtained with the optimized LDH catalyst CoFe35 presented in this work are comparable or even better than most published OER results for Co LDH-related catalysts.

10.1002/cssc.201601272

Table 1. Comparison of the electrocatalytic performance of CoFe35 with Co LDH-related catalysts reported in literature.

Sample	Current density at 10 mA/cm^2	Tafel slope	Electrolyte	Reference
	V vs. RHE	mV/dec		
CoFe35 LDH	1.58	49	0.1 M KOH	This work
CoZn LDH	~1.72*	-	0.1 M KOH	[36]
Exfol. Co LDH	1.58	45	1 M KOH	[37]
CoMn LDH	1.55	43	1 M KOH	[38]
CoFe LDH film	-	29	1 M KOH	[20]
CoO/Co_3O_4 nc	1.66	89	0.5 M KOH	[17]
LDH FeCo	1.56	85	1 M KOH	[39]
Gelled FeCoW	1.45	37	1 M KOH	

* Converted from the raw data based on NHE.

The long-term stability of the optimal CoFe35 catalyst was further investigated under conditions closer to application by a galvanostatic stability (GSS) test[40] in a flow-through cell at a current density of 10 mA/cm^2. The catalyst was deposited on a Ni foam electrode (1.0 × 1.0 cm^2) by means of spray coating with an optimized sample loading of 4.5 mg/cm^2. As shown in Figure 8, the iR-corrected potential applied to the working electrode at 10 mA/cm^2 is plotted as function of time. The potential during polarization of the electrode at 10 mA/cm^2 first decreased slightly from ca. 1.50 V vs. RHE in the first 1 h, then increased to ca. 1.51 V vs. RHE after 5 h. After that, it suddenly increased to ca. 1.53 V vs. RHE, which is probably due to the detachment of a part of the catalyst film from the electrode. Interestingly, after the initial deactivation processes within the first 5 h, the catalyst generally maintained stable performance afterwards with only minor fluctuations around 1.53 V vs. RHE. The changes in the ambient temperature contributed to the fluctuations of the potential curve in accordance with the diurnal cycle. In general, the CoFe35 catalyst exhibited very good stability in the OER in an alkaline electrolyte for at least 48 h.

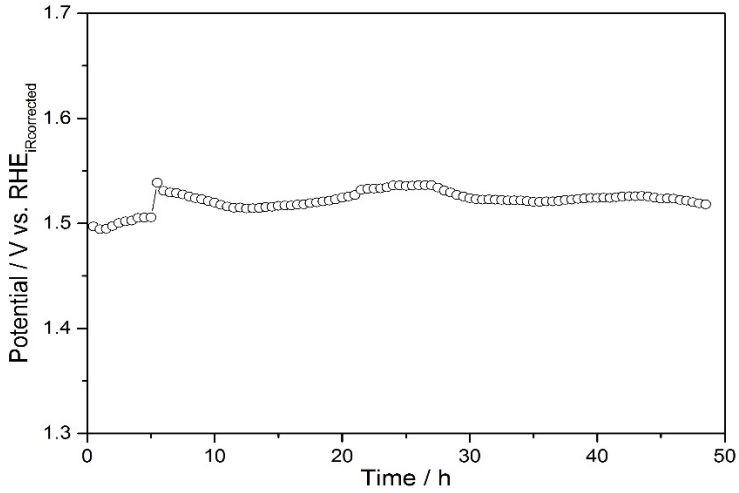

Figure 8. Long-term stability of CoFe35 during continuous polarization at 10 mA/cm^2 in a flow-through cell. The long-term stability test was performed in 1 M KOH electrolyte at room temperature on a 1 × 1 cm^2 Ni foam electrode sprayed-coated with an optimized sample loading of 4.5 mg/cm^2.

It is widely accepted that the incorporation of Fe dramatically improves the OER activity of Ni-based LDH catalysts.[31,32,41,42] Trotochaud et al.[41] showed that pure Ni-LDH catalysts without Fe exhibited very poor OER activity and, more importantly, Fe was found to be the only promising dopant exhibiting a synergistic effect on Ni among several redox-active metals.[42] Accordingly, it was proposed that Fe was the active site for the OER and the Ni-LDH acted as conductive support.[31] Similarly, it has been recently found that the inclusion of Fe in Co LDHs improved the OER activity.[20–22,39] Burke et al.[20] attributed the activity improvement to the same synergistic effect observed for NiFe LDHs. The Co LDH is assumed to provide a conductive host for Fe, which serves as the (most) active site for the OER.[20] However, unlike the Ni LDHs, Co LDH without Fe exhibits reasonable intrinsic activity for the OER, which emphasizes the potential synergistic effect between Co and Fe as two cooperating active sites.

Recently, using operando Mössbauer spectroscopy Chen et al.[43] observed that Fe^{4+} is present in the NiFe LDH catalyst during the whole OER-active potential range subsequent to the evolution of oxygen at about 1.62 V vs. RHE. The role of Fe^{4+} was, however, not fully elucidated in this study, because the presence of Fe^{4+} seemed to be consistent with both the "Ni active site" and the "Fe active site" mechanism. On the other hand, Co^{4+} species have been observed in OER-active catalysts under oxygen evolution conditions and are widely accepted to be a vital intermediate in the OER catalytic cycle by Co-based catalysts.[7,11,44] According to the OER pathway proposed by Ullmann et al.,[45] the Co^{4+} species coordinated

to oxo groups facilitate the proton-coupled electron transfer (PCET) steps leading to the formation of O• radicals on the Co^{3+} sites. It is well known that Fe is oxidized at lower potential than Co.[46] Therefore, Fe can substitute Co in the CoFe LDHs in forming oxo species at lower potentials, which may facilitate the PCET steps ultimately enhancing the overall OER catalysis.

Conclusions

Co-based layered double hydroxides were prepared by co-precipitation with Al^{3+} or Fe^{3+} ions. The extensive structural characterization confirmed that the LDH structure was successfully formed with Al^{3+} or Fe^{3+} ions in the range from 15 to 45 at%. The electrochemical studies showed that Al^{3+} suppressed the OER activity, whereas Fe^{3+} enhanced the activity with an optimum content of Fe amounting to 35 at%. The optimal $Co_{0.65}Fe_{0.35}(OH)_2$ catalyst showed very good long-term stability in 1 M KOH for at least 48 h. All results point to a synergistic effect between the Co and Fe ions in the LDH structure establishing a systematic basis for further research on Co- and Fe-containing LDHs as catalysts for the OER.

Acknowledgement

Financial support (SusHy: Grant 03X3581D) from the German Federal Ministry of Education and Research (BMBF) is gratefully acknowledged.

Experimental section

The catalysts were prepared by co-precipitation using $Co(NO_3)_2{\cdot}6H_2O$ (Sigma-Aldrich, 99.999 %), $Fe(NO_3)_3{\cdot}6H_2O$ (Sigma-Aldrich, 99.999 %), $Al(NO_3)_3{\cdot}9H_2O$ (Sigma-Aldrich, 99.997 %), NaOH (Sigma-Aldrich, 99.99 %), $Na_2CO_3{\cdot}10H_2O$ (Sigma-Aldrich, 99.999 %) and HPLC water without any further purification. For a common synthesis, 10 mL 5 mM $Co(NO_3)_2/Al(NO_3)_3$ or $Co(NO_3)_2/Fe(NO_3)_3$ aqueous solution was dropwise added into 50 mL water at 25°C within 30 min under rigorously stirring. At the same time, an alkaline solution containing 2 M NaOH and 0.3 M Na_2CO_3 was added to the solution via an autotitrator to maintain a pH of 9. After complete adding of salt solution, the brown suspension was further stirred at 25°C T for 2 h. After that, the precipitate was filtered and re-dispersed in 50 mL water three times. The resulting solid was dried at 30 °C in flowing air overnight and then finely ground in a mortar for further use.

The ICP-OES (PU701 UNICAM) was used to determine the metal content. The XRD patterns were recorded in a Philips X´Pert MPD system with Cu Kα irradiation and post-

conochromator in a 2θ range of 5° to 80°. The TG measurements were performed using a Cahn TG 2131 thermobalance coupled with a quadrupole mass spectrometer (QMS, Balzer, Omnistar). Typically, 20 mg of the samples were heated to 800 °C at a rate of 5 °C/min in 100 NmL/min 20 vol% O_2/He flow. The TPR experiments were performed by heating about 50 mg catalyst in a tubular reactor from 50 °C to 700 °C with a rate of 5 K/min in a tubular reactor. The H_2 content in the evolved gases was detected by a thermal conductivity detector (Xstream). The Raman spectra were recorded with a diffuse Raman spectrometer (iHR 550, HORIBA) using the 3.5 mW laser with the wavelength of 532 nm. The XPS measurements were carried out in an ultra-high vacuum set-up equipped with a monochromatic Al Kα X-ray source (1486.6 eV; anode operating at 14.5 kV and 35 mA) and a high resolution Gammadata-Scienta SES 2002 analyzer. The base pressure in the measurement chamber was maintained at about 7 $\times 10^{-10}$ mbar. The XP spectra were recorded in the fixed transmission mode with a pass energy of 200 eV. Charging effects were compensated by applying a flood gun. The fitting was performed with a minimum number of peaks using the CasaXPS software by limiting the peak positions and FWHMs to fixed binding energy ranges. All the XP spectra were calibrated by aliphatic carbon species at 284.5 eV.

The XAFS measurements were performed at the undulator beamline P65 of PETRA III storage ring operating at 6 GeV in top-up mode. The experiments were carried out in transmission mode at the Fe*K* (7112 eV) and Co*K* (7709 eV) edges. For each of the samples, multiple identical spectra were acquired and averaged to improve the signal-to-noise ratio. Initial processing of the XAFS data was performed using the program Athena.[47] EXAFS analysis was conducted in Artemis using the FEFF8 code[48] in order to extract coordination numbers (CN), interatomic distances (R), disorder parameters (Debye-Waller factors, σ^2) and edge energy shifts ΔE. The details of the EXAFS analysis are provided in the supplementary information (Tables S2 and S3).

GC RDE electrodes with a diameter of 3.8 mm were first polished on 1500 grid sand paper, and then on a polishing cloth with alumina pastes of different grain sizes (3-0.05 μm), and then rinsed in DI water for 15 min and subsequently in acetone for 5 min. The catalyst ink was prepared by dispersing 5 mg catalyst, 1 mg Vulcan XC-72 and 34 μL 5% Nafion in 1 mL H_2O:EtOH = 1:1 solution. Fort a given catalyst ink, 5.7 μL were dropped on the electrode and dried at room temperature under rotation at 500 rpm for 15 min. The resulting catalyst loading was 250 μg/cm^2. Six electrodes prepared from each ink were tested in a three-electrode system with Pt mesh as a counter electrode and an Orion™ 900200 Sure-Flow™ as the reference electrode. The electrolyte was 0.1 M KOH saturated with O_2. Electrochemical

impedance spectroscopy (EIS) was measured at the open circuit potential (OCP) from 500 kHz to 50 Hz with AC perturbation of 10 mV to determine the uncompensated resistance. Linear sweep voltammetry (LSV) was carried out between –0.5 V and 1.5 V vs. Ag/AgCl/3 M KCl reference electrode with a scan rate of 1 mV/s and rotation rate of 1600 rpm. Samples for long-term stability test were deposited on Ni foam electrodes ($1 \times 1 \times 0.15$ cm^3) by means of spray coating at 120 ^oC on a hot plate. The catalyst ink contained 250 mg catalyst, 28.3 ml EtOH, 20 ml H_2O and 1.7 ml 5% Nafion. The long-term stability test was performed in a flow-through cell controlled by a multichannel bio-logic VMP-3 potentiostat. The counter electrode was Ni foam ($1 \times 1 \times 0.3$ cm^3) while a Ag/AgCl/3M KCl / 1M KOH double junction electrode served as the reference electrode. For the OER half-cell measurement, the electrolyte (1 M KOH) pre-saturated by purging with O_2 was continuously pumped from the anolyte electrolyte reservoir through the flow-through cell. A second electrolyte reservoir, containing the catholyte (also 1 M KOH) for the counter reaction (HER), was pre-saturated by purging with Ar and pumped through the catholyte compartment of the cell. The anolyte and catholyte cell compartments were separated by FAAM-75-PK alkaline exchange membrane (FuMA-Tech, Germany), to prevent the mixing of H_2 and O_2. EIS was measured at the OCP from 50 kHz to 50 Hz with AC perturbation of 10 mV to determine the uncompensated resistance. Galvanodynamic sweep (GDS) was carried out between 0 mA and 10 mA at a scan rate of 1 mA/s during cycling the electrolyte, followed by chronopotentiometry (CPM) at 10 mA for 30 min. The number of cycles was 96, which corresponds to 48 h of the GSS test.

[1] T. R. Cook, D. K. Dogutan, S. Y. Reece, Y. Surendranath, T. S. Teets, D. G. Nocera, *Chem. Rev.* **2010**, *110*, 6474–6502.
[2] M. G. Walter, E. L. Warren, J. R. McKone, S. W. Boettcher, Q. Mi, E. A. Santori, N. S. Lewis, *Chem. Rev.* **2010**, *110*, 6446–6473.
[3] a) N. Danilovic et al., *J. Phys. Chem. Lett.* **2014**, *5*, 2474–2478; b) C. C. L. McCrory, S. Jung, J. C. Peters, T. F. Jaramillo, *J. Am. Chem. Soc.* **2013**, *135*, 16977–16987;
[4] J. Wang, W. Cui, Q. Liu, Z. Xing, A. M. Asiri, X. Sun, *Adv. Mater.* **2016**, *28*, 215–230.
[5] M. W. Kanan, D. G. Nocera, *Science* **2008**, *321*, 1072–1075.
[6] M. Risch, V. Khare, I. Zaharieva, L. Gerencser, P. Chernev, H. Dau, *J. Am. Chem. Soc.* **2009**, *131*, 6936–6937.
[7] J. G. McAlpin, Y. Surendranath, M. Dincă, T. A. Stich, S. A. Stoian, W. H. Casey, D. G. Nocera, R. D. Britt, *J. Am. Chem. Soc.* **2010**, *132*, 6882–6883.
[8] P. Du, O. Kokhan, K. W. Chapman, P. J. Chupas, D. M. Tiede, *J. Am. Chem. Soc.* **2012**, *134*, 11096–11099.
[9] C. L. Farrow, D. K. Bediako, Y. Surendranath, D. G. Nocera, S. J. L. Billinge, *J. Am. Chem. Soc.* **2013**, *135*, 6403–6406.
[10] K. Klingan, F. Ringleb, I. Zaharieva, J. Heidkamp, P. Chernev, D. Gonzalez-Flores, M. Risch, A. Fischer, H. Dau, *ChemSusChem* **2014**, *7*, 1301–1310.
[11] J. B. Gerken, J. G. McAlpin, J. Y. C. Chen, M. L. Rigsby, W. H. Casey, R. D. Britt, S. S. Stahl, *J. Am. Chem. Soc.* **2011**, *133*, 14431–14442.
[12] B. S. Yeo, A. T. Bell, *J. Am. Chem. Soc.* **2011**, *133*, 5587–5593.
[13] J. Bao, X. Zhang, B. Fan, J. Zhang, M. Zhou, W. Yang, X. Hu, H. Wang, B. Pan, Y. Xie, *Angew. Chem. Int. Ed.* **2015**, *54*, 7399–7404.
[14] L. Xu, Q. Jiang, Z. Xiao, X. Li, J. Huo, S. Wang, L. Dai, *Angew. Chem. Int. Ed.* **2016**, *55*, 5277–5281.
[15] H.-Y. Wang, S.-F. Hung, H.-Y. Chen, T.-S. Chan, H. M. Chen, B. Liu, *J. Am. Chem. Soc.* **2016**, *138*, 36–39.
[16] D. González-Flores, I. Sánchez, I. Zaharieva, K. Klingan, J. Heidkamp, P. Chernev, P. W. Menezes, M. Driess, H. Dau, M. L. Montero, *Angew. Chem. Int. Ed.* **2015**, *54*, 2472–2476.
[17] C.-W. Tung, Y.-Y. Hsu, Y.-P. Shen, Y. Zheng, T.-S. Chan, H.-S. Sheu, Y.-C. Cheng, H. M. Chen, *Nat. Commun.* **2015**, *6*, 8106.
[18] K. J. May, C. E. Carlton, K. A. Stoerzinger, M. Risch, J. Suntivich, Y.-L. Lee, A. Grimaud, Y. Shao-Horn, *J. Phys. Chem. Lett.* **2012**, *3*, 3264–3270.
[19] A. Bergmann, E. Martinez-Moreno, D. Teschner, P. Chernev, M. Gliech, J. F. de Araújo, T. Reier, H. Dau, P. Strasser, *Nat. Commun.* **2015**, *6*, 8625.
[20] M. S. Burke, M. G. Kast, L. Trotochaud, A. M. Smith, S. W. Boettcher, *J. Am. Chem. Soc.* **2015**, *137*, 3638–3648.
[21] C. G. Morales-Guio, L. Liardet, X. Hu, *J. Am. Chem. Soc.* **2016**, *138*, 8946–8957.
[22] Y. Vlamidis, E. Scavetta, M. Gazzano, D. Tonelli, *Electrochim. Acta* **2016**, *188*, 653–660.
[23] Z. Liu, R. Ma, M. Osada, K. Takada, T. Sasaki, *J. Am. Chem. Soc.* **2005**, *127*, 13869–13874.
[24] J. Pérez-Ramírez, G. Mul, F. Kapteijn, J. A. Moulijn, *J. Mater. Chem.* **2001**, *11*, 821–830.
[25] J. Yang, H. Liu, W. N. Martens, R. L. Frost, *J. Phys. Chem. C* **2010**, *114*, 111–119.
[26] J. Pérez-Ramírez, G. Mul, J. Moulijn, *Vib. Spectrosc.* **2001**, *27*, 75–88.
[27] S. Velu, K. Suzuki, M. P. Kapoor, S. Tomura, F. Ohashi, T. Osaki, *Chem. Mater.* **2000**, *12*, 719–730.
[28] a) J. A. Díaz, H. Akhavan, A. Romero, A. M. Garcia-Minguillan, R. Romero, A. Giroir-Fendler, J. L. Valverde, *Fuel Process. Technol.* **2014**, *128*, 417–424; b) A.

Griboval-Constant, A. Butel, V. V. Ordomsky, P. A. Chernavskii, A. Y. Khodakov, *Appl. Catal., A* **2014**, *481*, 116–126;
[29] A. P. Grosvenor, B. A. Kobe, M. C. Biesinger, N. S. McIntyre, *Surf. Interface Anal.* **2004**, *36*, 1564–1574.
[30] M. Wilke, F. Farges, P.-E. Petit, G. E. Brown, F. Martin, *Am. Mineral.* **2001**, *86*, 714–730.
[31] D. Friebel et al., *J. Am. Chem. Soc.* **2015**, *137*, 1305–1313.
[32] M. Gorlin, P. Chernev, J. Ferreira de Araujo, T. Reier, S. Dresp, B. Paul, R. Krahnert, H. Dau, P. Strasser, *J. Am. Chem. Soc.* **2016**, *138*, 5603–5614.
[33] R. W. G. Wyckoff, *Crystal structures* **1963**, 239–444.
[34] a) W. P. Weulfing, S. J. Green, J. J. Pietron, D. E. Cliffel, R. W. Murray, *J. Am. Chem. Soc.* **2000**, *122*, 11465–11472; b) J. E. Katz, X. Zhang, K. Attenkofer, K. W. Chapman, C. Frandsen, P. Zarzycki, K. M. Rosso, R. W. Falcone, G. A. Waychunas, B. Gilbert, *Science* **2012**, *337*, 1200–1203;
[35] N. Lu, L. Li, W. Banerjee, P. Sun, N. Gao, M. Liu, *J. Appl. Phys.* **2015**, *118*, 45701.
[36] X. Zou, A. Goswami, T. Asefa, *J. Am. Chem. Soc.* **2013**, *135*, 17242–17245.
[37] F. Song, X. Hu, *Nat. Commun.* **2014**, *5*, 4477
[38] F. Song, X. Hu, *J. Am. Chem. Soc.* **2014**, *136*, 16481–16484.
[39] B. Zhang et al., *Science* **2016**, *352*, 333–337.
[40] A. Maljusch, O. Conradi, S. Hoch, M. Blug, W. Schuhmann, *Anal. Chem.* **2016**, *88*, 7597–7602.
[41] L. Trotochaud, S. L. Young, J. K. Ranney, S. W. Boettcher, *J. Am. Chem. Soc.* **2014**, *136*, 6744–6753.
[42] L. J. Enman, M. S. Burke, A. S. Batchellor, S. W. Boettcher, *ACS Catal.* **2016**, *6*, 2416–2423.
[43] J. Y. C. Chen, L. Dang, H. Liang, W. Bi, J. B. Gerken, S. Jin, E. E. Alp, S. S. Stahl, *J. Am. Chem. Soc.* **2015**, *137*, 15090–15093.
[44] M. W. Kanan, J. Yano, Y. Surendranath, M. Dinca, V. K. Yachandra, D. G. Nocera, *J. Am. Chem. Soc.* **2010**, *132*, 13692–13701.
[45] A. M. Ullman, C. N. Brodsky, N. Li, S.-L. Zheng, D. G. Nocera, *J. Am. Chem. Soc.* **2016**, *138*, 4229–4236.
[46] A. J. Bard, L. R. Faulkner, *Electrochemical Methods: Fundamentals and Applications*, 2nd ed., John Wiley, New York, Chichester, **2001**.
[47] B. Ravel, M. Newville, *J. Synchrotron Radiat.* **2005**, *12*, 537–541.
[48] A. L. Ankudinov, B. Ravel, J. J. Rehr, S. D. Conradson, *Phys. Rev. B* **1998**, *58*, 7565–7576.